Material-minimizing forms and structures

MARTIN KILIAN*, Vienna University of Technology
DAVIDE PELLIS*, Vienna University of Technology
JOHANNES WALLNER, Graz University of Technology
HELMUT POTTMANN, Vienna University of Technology

Three-dimensional structures in building construction and architecture are realized with conflicting goals in mind: engineering considerations and financial constraints easily are at odds with creative aims. It would therefore be very beneficial if optimization and side conditions involving statics and geometry could play a role already in early stages of design, and could be incorporated in design tools in an unobtrusive and interactive way. This paper, which is concerned with a prominent class of structures, is a substantial step towards this goal. We combine the classical work of Maxwell, Michell, and Airy with differential-geometric considerations and obtain a geometric understanding of "optimality" of surface-like lightweight structures. It turns out that total absolute curvature plays an important role. We enable the modeling of structures of minimal weight which in addition have properties relevant for building construction and design, like planar panels, dominance of axial forces over bending, and geometric alignment constraints.

CCS Concepts: • **Computing methodologies** → **Shape modeling**; *Optimization algorithms*;

Additional Key Words and Phrases: computational design, minimum weight, material economy, truss-like continuum, architectural geometry, stress potential, total absolute curvature

ACM Reference Format:
Martin Kilian, Davide Pellis, Johannes Wallner, and Helmut Pottmann. 2017. Material-minimizing forms and structures. *ACM Trans. Graph.* 36, 6, Article 173 (November 2017), 12 pages.
https://doi.org/10.1145/3130800.3130827

1 INTRODUCTION

Motivation. A long-term goal in the design of forms and structures for architecture are design tools which assist the user in modeling geometric shapes, while automatically taking into account manufacturing, statics, material economy, and other aspects which have implications on buildability and cost. Even small steps towards this goal can shorten the *design loop*, where classically an act of design is followed by analysis, feedback to the designer, and another round of the loop. Specific to freeform architecture, a design tool able to take statics into account does not replace the full blown statics analysis required by law, but is able to reduce the number of iterations and thus significantly diminish the overall time needed for the final design. A tool sensitive to material economy and weight can have significant impact on building costs and may thus help to stay within the budget even for a geometrically complex structure. The present paper is a contribution to reach this long-term goal which in its full generality seems out of reach at the moment.

This paper tackles forms featuring prominently in freeform architecture, namely wide-span surface-like and lightweight structures. The word *shell* is sometimes employed here, cf. [Adriaenssens et al. 2014], but it does not necessarily refer to the specific mathematical model in structural engineering which goes under *shell*. Our implementation assists the design of such freeform structures by giving quick information on statics, material economy, and in part also manufacturing.

Several previous contributions to architectural geometry have already resulted in real projects, cf. the survey [Pottmann et al. 2015]. E.g. the *Armadillo Vault* Biennale exhibit by Ph. Block is connected to research on freeform masonry, and the roof of the Chadstone shopping centre in Melbourne corresponds to work on torsion-free support structures and quad meshes with planar faces. Like that previous work, our paper is intended to provide an algorithmic tool for architects, bringing us closer towards the long-term goal of computational design mentioned earlier.

Previous Work. This paper revolves around the problem of finding structures experiencing certain loads, which have minimal volume while stresses do not exceed certain limits. The most important and original contribution to this subject is by A.G.M. Michell [1904],

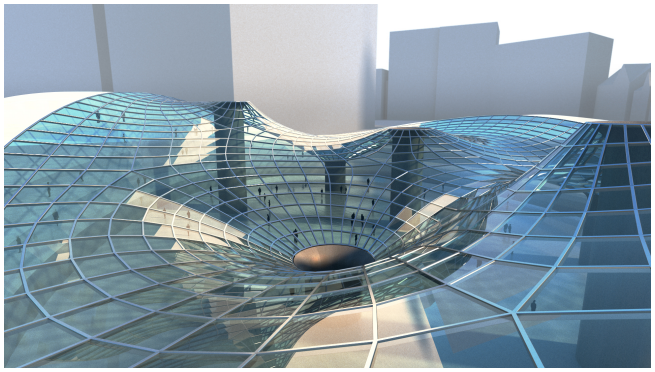

Fig. 1. We provide a tool for freeform architectural design that performs a combined form and stress optimization with the goal to create structures of minimal weight. We incorporate features relevant to statics (alignment of principal stress directions with principal curvature lines, local and global optimality properties regarding volume) and features relevant to architectural design like flat panels and the alignment of principal curves with the boundary. The workflow generating this example is shown by Figure 6.

*joint first authors

0730-0301/2017/11-ART173 $15.00
https://doi.org/10.1145/3130800.3130827

who studied optimal *trusses* and truss-like continua subject to constant external forces. His work is considered to be ahead of its time. Follow-up publications treat variations of the viewpoint (e.g. allowable strains instead of stresses, discrete trusses instead of continua) and further investigations in geometric properties of optimal trusses. E.g. Prager [1978] derives a discrete "Hencky-Prandtl" property of optimal trusses from limit strain considerations. Baker et al. [2013] study optimality in connection with Maxwell's reciprocal force diagrams and discuss primal/dual pairs of optimal trusses. There have also been clarifications and justifications [Goetschel 1981], and most importantly, the embedding of the original work into the systematic theory of optimization [Whittle 2007]. Recently A.G.M. Michell's work has been extended to shell-like structures by T. Mitchell [2013; 2014], where Michell's original constant force assumption is no longer valid. The present paper is also concerned with this topic. We should emphasize that in our search for optimal structures, the combinatorics of the structure is part of the solution. This aspect seems to have been neglected in the geometry processing community so far. E.g. Jiang et al. [2017] optimize space frames (not shells), keeping the combinatorics unchanged.

Imposing optimality properties on structures may not only influence the layout and combinatorics of the structure, but also the shape of the surface which the structure follows. This leads to *computational optimization as form-finding*. This principle is not new, cf. [Bletzinger and Ramm 1993]. We apply it to wide-span surface-like structures, which was first done by T. Mitchell [2013]. We compute surfaces where *principal curvature directions coincide with principal stress directions* and equivalently, meshes endowed with equilibrium forces which are principal. Such meshes represent structures where the "flow of forces" can be given a rigorous meaning. There seems to be no previous work on that specific topic, with the exception of [Schiftner and Balzer 2010] where planar-quad remeshing is guided by principal stress directions.

Our investigations feature a significant detail, namely the decoupling of horizontal and vertical stress components. This allows us to utilize *thrust networks* [Adriaenssens et al. 2014; Block and Ochsendorf 2007; de Goes et al. 2013; Panozzo et al. 2013] and the corresponding polyhedral stress potential as a finite element discretization, see [Fraternali 2010]. The resulting connections of statics with discrete differential geometry have already been exploited by Vouga et al. [2012].

Contributions of the present paper. After a recap of know material (Maxwell lemma, Michell's theorem, reciprocal force diagrams, Airy potential) we present new results on 2D optimal trusses, starting with relations between discrete curvatures of an Airy potential on the one hand, and the total volume of a truss on the other hand. This topic is interesting because of its connection to differential geometry and because it is relevant to applications, despite the restriction to 2D. An interesting point here is that the combinatorics of optimal structures is part of the solution.

We continue with optimal structures which represent three-dimensional freeform shells (in the broad meaning of the word). This topic is a bit more involved than the 2D case, but we are able to exploit analogies. We derive a procedure for optimization as well as theoretical insights on principal meshes in equilibrium.

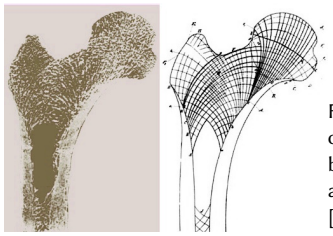

Fig. 2. Force-induced growth of bones obeys Michell's theorem as stated by Prop. 3: compression members and tension members are orthogonal [Wolff 1892].

The actual computation of optimal structures is not based on the discrete structure itself (this would be difficult, since the combinatorics of the solution is not known in advance), but consists of optimizing a continuous truss-like structure, followed by discretization. The methods employed in optimization are based on the constraint solver by Tang et al. [2014].

As to theory, we point out a connection between volume optimization and minimizing total absolute curvature. This connection could be very valuable for future research in various directions.

2 GEOMETRY OF FORCES

This section starts with two classical results, namely Michell's theorem on volume-optimal structures, and the existence of the Airy stress potential (both the discrete case and the continuous case). We continue with establishing a relation between minimization of volume on the one hand, and minimization of total curvature on the other hand. The greater part of this section applies to two-dimensional structures. The 2D case is the basis of the 3D case, but is also interesting in its own right. This is due to its relation to differential geometry, and to potential applications: Finding volume-minimal trusses is related to *topology optimization* which is relevant e.g. in 3D printing [Aage et al. 2015].

2.1 Maxwell's lemma and Michell's theorem

Forces, stresses, and volumes of trusses. We consider truss structures (both two- and three-dimensional) which are made of individual straight members connected together with joints that do not transfer any torque, i.e., the external load applied to an individual member consists of two opposite forces applied at either end. Tensile resp. compressive forces are positive resp. negative. For each member, we have the variables

$$\begin{aligned} &\text{length} \ldots\ldots\ldots\ldots\ldots\ \ell \\ &\text{cross-section area} \ldots\ldots\ a \\ &\text{force} \ldots\ldots\ldots\ldots\ldots\ f \\ &\text{stress} \ldots\ldots\ldots\ldots\ldots\ \sigma \end{aligned}$$

and the following relations between them:

$$\sigma = \frac{f}{a} \implies v = a\ell = \frac{f\ell}{\sigma}.$$

We assume that a linear-elastic material with limit stresses $\sigma^{\min} < 0$, $\sigma^{\max} > 0$ is used. Failure is excluded if $\sigma^{\min} \le \sigma \le \sigma^{\max}$. A member is fully stressed, if $\sigma = \sigma^{\min}$ (compression case) or $\sigma = \sigma^{\max}$ (tension case). We begin by stating a result which in this context is referred to as Maxwell's lemma:

Prop. 1. [Maxwell 1872]. *For any truss, the sum $\sum f\ell$ over all members equals a constant "$\mathcal{C}$" which only depends on the external*

load, and does not depend on the combinatorics and geometry of the truss itself.

The "external load" mentioned here and elsewhere in the paper includes boundary tractions. The proof is not obvious, but elementary, see e.g. [Parkes 1965, § 5.1]. Our principal interest is structures of *minimal volume* under prescribed load conditions and prescribed foundation points. Maxwell's lemma is relevant here because it is actually about volumes (note that $\sum f\ell = \sum v\sigma$). The most famous result concerning optimal structures is Michell's theorem:

Prop. 2. [Michell 1904]. *All members of a volume-optimal truss are fully stressed, and the total volume of all members equals*

$$v^{\text{total}} = \sum_{\text{members}} v = \sum_{\text{members}} a\ell = \frac{1}{\sigma^{\max}} \sum_{\substack{\text{tension}\\ \text{members}}} |f|\,\ell + \frac{1}{|\sigma^{\min}|} \sum_{\substack{\text{compression}\\ \text{members}}} |f|\,\ell.$$

Minimizing volume is equivalent to minimizing

$$\sum_{\text{members}} |f|\,\ell = \sum_{\substack{\text{tension}\\ \text{members}}} f\,\ell - \sum_{\substack{\text{compression}\\ \text{members}}} f\,\ell. \tag{1}$$

The statement about members being fully stressed is made plausible by the argument that a member which is not fully stressed can be replaced by a thinner one which is, thus reducing volume. This argument is faulty, however, because in the hyperstatic (statically indeterminate) case, modification of one member changes stresses in all members. See [Goetschel 1981] for a thorough discussion.

The equivalence stated above follows from Maxwell's lemma $\sum f\ell = C$: Instead of minimizing v^{total}, Michell [1904] proposes to minimize $\frac{2|\sigma^{\min}\sigma^{\max}|}{\sigma^{\max}-\sigma^{\min}} v^{\text{total}} + \frac{\sigma^{\max}+\sigma^{\min}}{\sigma^{\max}-\sigma^{\min}} C$ instead, which is equivalent. Expanding this expression miraculously yields $\sum |f|\ell$.

Stresses and volumes of a continuum. The engineering literature, starting with Michell [1904], considers continuous truss-like structures consisting of infinitely many infinitesimal members, see e.g. [Steigmann and Pipkin 1991]. The present paper implicitly uses that kind of continuum as well, switching back and forth between the discrete and the continuous cases. The purpose of the truss-like continuum is not to describe materials existing in reality, but to provide a continuous approximation of the discrete situation. A continuous version of Michell's theorem can be expressed in non-mathematical language as follows:

Prop. 3. [Whittle 2007, Th. 7.5]. *In a continuum (truss-like structure with infinitesimal members) which is volume-optimal under given external loads, all members are fully stressed. If tension members meet compression members, they must do so at right angles.*

Figure 2 illustrates the remarkable fact that natural structures appear to obey Michell's theorem if their growth is governed by the forces they experience (for bones, this is called Wolff's law).

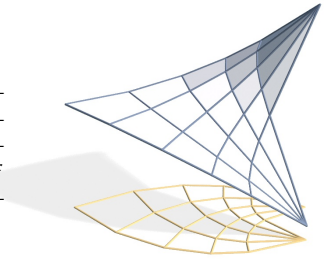

Fig. 3. The mesh yielding a volume-optimal truss (shown in yellow) together with the Airy polyhedron projecting onto it (blue). The angle of transverse mesh polylines enjoys a discrete Hencky-Prandtl property.

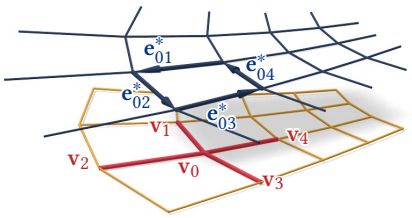

Fig. 4. A primal truss (yellow) and the dual-reciprocal truss (blue) whose edge vectors $\mathbf{e}^*_{ij}$ are constructed from the forces $\mathbf{f}_{ij}$ in the primal truss by rotating them by 90° (the missing edges correspond to external forces acting on boundary nodes).

Combinatorics and geometry of optimal discrete structures. The orthogonality of members mentioned in Prop. 3 does not strictly apply to the discrete case, but has to be taken into account if discrete structures are intended to approximate continuous ones. In particular, orthogonality between tension members and compression members suggests that optimal trusses have *quad mesh* combinatorics.

In the planar (2D) continuous case, even stronger conditions are true: The members form a *Hencky-Prandtl net*: any tension curve crossing two given compression curves turns through a constant angle, and vice versa, see [Whittle 2007, Th. 7.6] In the discrete case, only a weaker version of this statement holds. We cannot prove that all optimal trusses enjoy a discrete Hencky-Prandtl property, but this property does occur in optimal structures, see Fig. 3 and [Baker et al. 2013; Prager 1978]. Further, Mitchell [2013, §10.1] argues that in a volume-optimal 2D quad mesh, all faces have a circumcircle. This is seen by connecting volume-minimization with maximizing the area of faces, and deriving circularity from that.

The modern view of Michell's results. In this paper we need only the original mechanical engineering interpretation of A.G.M. Michell's seminal paper [1904]. His work has been re-examined frequently, in particular from the viewpoint of optimization. It turns out that the primal and dual versions of the problem statement correspond to minimizing volume under stress constraints, and maximizing work under deformation constraints, respectively. Modern treatments like [Whittle 2007] are not restricted to *volume* as optimization target, and besides limit stresses include other failure criteria like buckling.

2.2 Forces and discrete curvatures

This section starts with the well known geometric relation between a 2D truss and its dual-reciprocal truss whose members are the forces acting in the first truss. This construction is due to Maxwell [1872] and is the basis of the *thrust network* method which among others has been employed to analyze and design freeform masonry [Block and Ochsendorf 2007; de Goes et al. 2013; Panozzo et al. 2013; Vouga et al. 2012].

Reciprocal diagrams of members and forces. Consider a two-dimensional truss in the xy plane whose members are the edges of a mesh (V, E, F). An oriented edge can be written as a pair of vertices $\mathbf{v}_i\mathbf{v}_j$, but also an intersection of faces $f_k \cap f_l$, where f_k lies to the left and f_l to the right. The boundary of a face $\mathbf{v}_{i_1} \ldots \mathbf{v}_{i_n}$ is a cycle

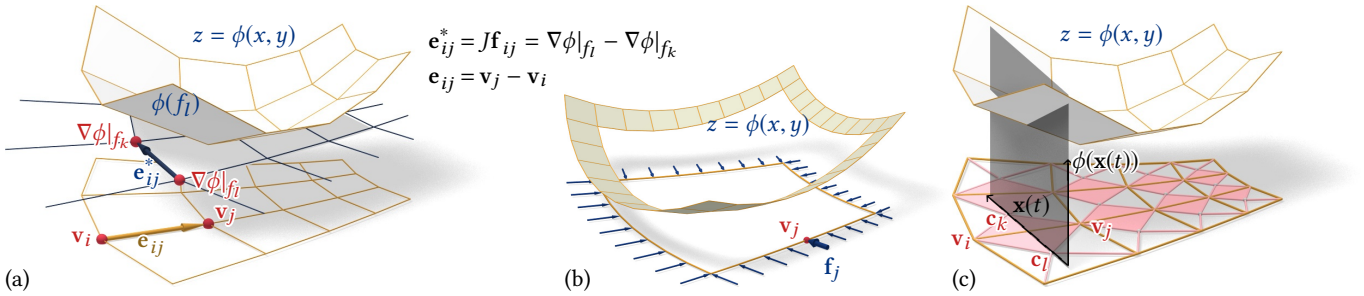

Fig. 5. *Airy polyhedra of trusses.* (a) An Airy polyhedron "$z = \phi(x, y)$" which projects onto the primal truss. The gradients of the piecewise-linear function ϕ are the vertices of a dual-reciprocal truss – compare with Fig. 4. (b) Given forces along the polygonal boundary of a planar domain, we incrementally construct the boundary strip of an Airy polyhedron by relating its face gradients with the given forces. Equilibrium ensures the construction closes up. (c) The Airy potential $\phi(\mathbf{x}(t))$ experiences a kink a point $\mathbf{x}(t)$ moves across the edge $\mathbf{v}_i\mathbf{v}_j$ at right angles. The kink is of magnitude $\|\mathbf{f}_{ij}\| = \|\mathbf{e}^*_{ij}\|$. This figure also illustrates the quadrilateral $\mathbf{v}_i\mathbf{c}_l\mathbf{v}_j\mathbf{c}_k$ which serves as region of influence of the member $\mathbf{v}_i\mathbf{v}_j$.

of oriented edges, with edge vectors summing up to zero:

$$\mathbf{e}_{i_1 i_2} + \mathbf{e}_{i_2 i_3} + \cdots + \mathbf{e}_{i_n i_1} = \mathbf{o}. \tag{2}$$

The force exerted on the node $\mathbf{v}_i$ by the member $\mathbf{v}_i\mathbf{v}_j$ is denoted by $\mathbf{f}_{ij}$, and we have $\mathbf{f}_{ji} = -\mathbf{f}_{ij}$. If $\mathbf{v}_i\mathbf{v}_{j_1}, \ldots \mathbf{v}_i\mathbf{v}_{j_m}$ are the edges emanating from $\mathbf{v}_i$ (in counterclockwise order), then equilibrium of the forces acting on $\mathbf{v}_i$ is expressed as

$$\mathbf{f}_{i,j_1} + \mathbf{f}_{i,j_2} \cdots + \mathbf{f}_{i,j_m} = \mathbf{o}. \tag{3}$$

This means that vectors $\mathbf{f}_{i,j_r}$ are the edge vectors of the boundary of a "dual" face. For better visualization, we rotate the dual mesh by 90°, letting $\mathbf{e}^*_{ij} = J\mathbf{f}_{ij}$. The symbol J refers to rotation in the xy plane and is expressed by multiplication with the matrix $\left(\begin{smallmatrix} 0 & -1 \\ 1 & 0 \end{smallmatrix}\right)$. Equation (3) translates to

$$\mathbf{e}^*_{i,j_1} + \mathbf{e}^*_{i,j_2} \cdots + \mathbf{e}^*_{i,j_m} = \mathbf{o}, \tag{4}$$

which is a closure condition analogous to (2). In fact, if the primal mesh (V, E, F) is simply connected, there exists a dual mesh (V^*, E^*, F^*), where primal vertices, edges, faces corresponds to dual faces, edges, vertices, respectively. Dual edges are rotated forces which act in the primal edges, see Fig. 4.

The Airy potential. It is known that a reciprocal pair of trusses gives rise to a polyhedral surface which can be written as graph of a piecewise-linear function, $z = \phi(x, y)$. Its vertices and edges project onto the nodes and members of the primal truss, while the gradient of ϕ in a face equals the dual vertex corresponding to that face, see [Ash et al. 1988] and Figures 3, 5a. If the truss is not simply connected, the Airy polyhedron exists only locally.

In the 2D continuous case, consider a stress field in a domain D. We use the usual notation for the stress tensor,

$$S = \begin{pmatrix} \sigma_{xx} & \sigma_{xy} \\ \sigma_{xy} & \sigma_{yy} \end{pmatrix}.$$

Static equilibrium is expressed by $\operatorname{div} S = 0$, where the divergence is applied to both columns separately. This condition implies local existence of an Airy potential $\phi(x, y)$ such that

$$\nabla^2\phi = \begin{pmatrix} \phi_{,xx} & \phi_{,xy} \\ \phi_{,xy} & \phi_{,yy} \end{pmatrix} = \hat{S} = \begin{pmatrix} \sigma_{yy} & -\sigma_{xy} \\ -\sigma_{xy} & \sigma_{xx} \end{pmatrix}, \tag{5}$$

where derivatives are indicated by a comma and subscripts. If D is simply connected, ϕ exists globally. Fraternali [2010] discusses how Airy polyhedra can be seen as a certain finite element discretization of continuous stress potentials. See also [Miki et al. 2015; Vouga et al. 2012] for further details.

Connection between kinks and volumes. We use the discrete Airy potential to establish a first new relation between volumes and discrete curvatures. Having in mind the properties of continuous optimal structures (see in particular Prop. 3), we consider *circular quad meshes*. The geometric setting appropriate to our situation is 3D *isotropic geometry*, where the slope of a line w.r.t. the horizontal xy plane plays the role of an angle, and change in slope (such as a 2nd derivative, or a kink divided by horizontal length) plays the role of curvature [Pottmann and Liu 2007]. We need the following ingredients:

- For a member $\mathbf{v}_i\mathbf{v}_j$, the product $|f| \cdot \ell$ (force times length) is expressed as $\|\mathbf{e}_{ij}\| \cdot \|\mathbf{e}^*_{ij}\|$, by construction of the dual truss.
- We define a region of influence of this member, namely the quadrilateral $\mathbf{v}_i\mathbf{c}_k\mathbf{v}_j\mathbf{c}_l$, where $\mathbf{c}_k, \mathbf{c}_l$ are circumcenters of faces adjacent to the member, see Fig. 5c. Its area is $area_{ij}$.
- The kink in the Airy potential along a line which crosses this member at right angles, equals $\pm\|\nabla\phi|_{f_k} - \nabla\phi|_{f_l}\|$ by definition of ∇. It equals $\pm\|\mathbf{e}^*_{ij}\|$ by construction of the potential.
- The isotropic curvature of the Airy potential surface across the edge $\mathbf{v}_i\mathbf{v}_j$ is the kink divided by the distance of centers $\mathbf{c}_k, \mathbf{c}_l$. We temporarily call this value $curvature_{ij}$.

Putting everything together, we get

$$\begin{aligned} \sum_{\text{members}} |f|\,\ell &= \sum\nolimits_{\mathbf{v}_i\mathbf{v}_j \in E} \|\mathbf{e}^*_{ij}\|\,\|\mathbf{e}_{ij}\| \\ &= \sum\nolimits_{\mathbf{v}_i\mathbf{v}_j = f_k \cap f_l \in E} \|\mathbf{e}_{ij}\|\,\|\mathbf{c}_k - \mathbf{c}_l\|\,\frac{\|\mathbf{e}^*_{ij}\|}{\|\mathbf{c}_k - \mathbf{c}_l\|} \\ &= \sum\nolimits_{\mathbf{v}_i\mathbf{v}_j \in E} 2\,\text{area}_{ij} \cdot |\text{curvature}_{ij}|. \end{aligned} \tag{6}$$

Except for the boundary, the areas of influence cover the mesh, so we have converted the volume optimization problem "$\sum |f|\ell \to \min$" into a total curvature minimization problem. It remains to interpret the formula above and give it a meaning in terms of classical differential geometry.

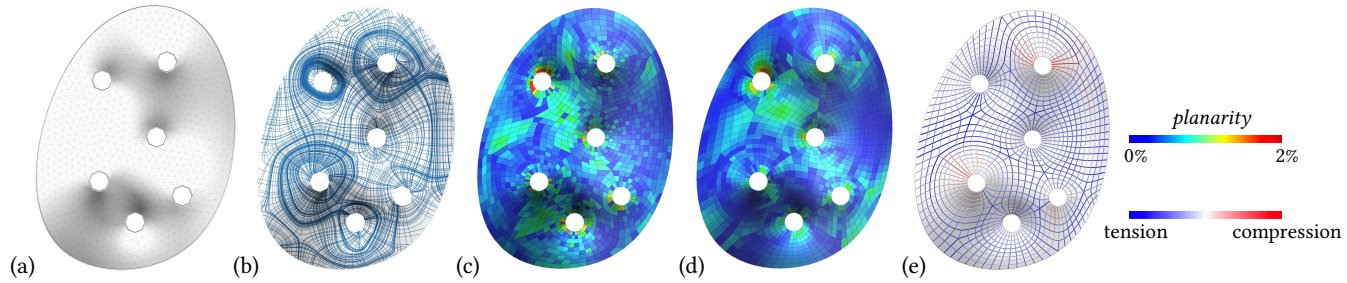

Fig. 6. *Workflow for optimizing structures.* We start with a boundary curve and compute the optimal stress potential $\phi(x, y)$ and design surface $s(x, y)$ shown in (a). Optimization in particular makes the principal stress directions coincide with the principal curvature directions (b), so a quad mesh which follows these directions has approximately planar faces and is optimally placed to carry the flow of forces (c). The measure of planarity of individual quads given here is the ratio of distance of diagonals, over average edge length. Optimization towards planarity and equilibrium does not change the mesh much (d), verifying that the 'continuum' version of the optimization has been accurate. Finally we construct a structure following the mesh, connecting members with rigid joints. Finite element analysis shows both tension and compression in its members (e).

Total isotropic curvature. Isotropic geometry is a linearization of Euclidean geometry with a distinguished vertical z axis and a horizontal xy plane. Surfaces are described as graphs $z = \phi(x, y)$, and the role of the second fundamental form is played by the Hessian of ϕ. Its eigenvalues are *i*-principal curvatures, and its eigenvectors define the *i*-principal directions and the network of *i*-principal curves. This network of curves is *i*-orthogonal, meaning that its projection onto the xy plane is an orthogonal network of curves. Like the classical Euclidean principal curves, the *i*-curves form a *conjugate* network. For details we refer to [Pottmann and Liu 2007].

Discretizations of conjugate networks are planar quad meshes [Bobenko and Suris 2009; Liu et al. 2006]. A *principal* curve network, characterized by conjugacy+orthogonality, requires that a discrete version of orthogonality is imposed on top of conjugacy; such a net thus is discretized as a *circular* quad mesh in the classical case, and as an *i*-circular mesh in the isotropic case: an *i*-circular mesh is a quad mesh with planar faces whose projection onto the xy plane is a 2D circular net [Pottmann and Liu 2007]. The Airy polyhedra erected over 2D circular nets are therefore discretizations of *i*-principal curve networks.

We now think of a sequence of finer and finer Airy polyhedra which converge to a principal parametrization of a continuous Airy potential $\phi(x, y)$, see [Bobenko and Suris 2009, § 5.6], and we investigate the limit of Equ. (6): In isotropic geometry, curvature measures the change in slope w.r.t. progress in the xy plane (i.e., *i*-curvature is a second derivative of the z coordinate w.r.t. arc length in the xy plane). Thus, a discrete version of *i*-curvature is the value "$curvature_{ij}$" used above (it is a kink divided by a horizontal length). Curvatures along the *i*-principal directions are the *i*-principal curvatures κ_1, κ_2. Since our limit of circular meshes is principal parametrization, we see that Equation (6) discretizes the integral $2\int(|\kappa_1| + |\kappa_2|)\,dxdy$. We summarize this result:

Prop. 4. *The infinitesimal members of a volume-minimizing optimal truss-like continuum are aligned with the isotropic-principal directions of the Airy potential surface $z = \phi(x, y)$, which minimizes total absolute curvature, i.e,*

$$\int (|\kappa_1| + |\kappa_2|)\,dxdy \to \min,$$

under the given boundary and load conditions. A volume-minimizing discrete truss — if orthogonality is enforced by means of the circular property — are found as projections of a polyhedral Airy potential minimizing a discrete version of total absolute curvature (again, under the given boundary and load conditions):

$$\sum_{\text{members } \mathbf{v}_i\mathbf{v}_j} |\text{curvature}_{ij}| \cdot \text{area}_{ij} \to \min .$$

It is not difficult to see that κ_1, κ_2 equal the principal stresses, which has already been noticed by [Strubecker 1962]. We will see that in the 3D (shell) case, an analogous result holds, see Equ. (16).

2.3 Computing optimal trusses in 2D

We are now able to solve the following problem: *Given is a polygonal domain D in $\mathbb{R}^2$ with vertices $\mathbf{v}_1, \ldots, \mathbf{v}_n$. Further we are given forces $\mathbf{f}_j$ acting on $\mathbf{v}_j$ which are in equilibrium (i.e., there is zero net force and zero net torque). Connect the given vertices by a truss in the interior of D which balances the given forces in a volume-optimizing manner.* A four-step procedure determines the combinatorics and geometry of the solution:

(1) The given loads define an Airy potential $\phi(x, y)$ outside D.
(2) Extend $\phi(x, y)$ to the interior of D, minimizing $\int |\kappa_1| + |\kappa_2|$, see Fig. 7.
(3) Find an *i*-circular net approximating the surface $z = \phi(x, y)$.
(4) In theory, this net projects onto an optimal truss. In order to account for discretization errors, apply a final round of direct optimization to this truss.

Step 1 is illustrated by Fig. 5b. A piecewise-linear Airy potential $\phi(x, y)$ in a neighbourhood of D just outside the boundary ∂D is composed of linear functions $\phi^j(\mathbf{x}) = \langle \nabla\phi^j, \mathbf{x}\rangle + \gamma_j$, whose domain is bounded by the edge $\mathbf{v}_j\mathbf{v}_{j+1}$, and the lines of action of the forces $\mathbf{f}_j$ and $\mathbf{f}_{j+1}$ (indices modulo n). The Airy potential is unique only up to adding a linear function, so we let $\nabla\phi^1 = \mathbf{o}$, $\gamma_1 = 0$. Since ϕ^{j-1}, ϕ^j have the same value for the vertex $\mathbf{v}_j$, and § 2.2 implies that $\nabla\phi^j = \nabla\phi^{j-1} + J\mathbf{f}_j$, we recursively define $\phi^2, \phi^3, \ldots$ Our equilibrium assumption ensures that $\phi^{n+1} = \phi^1$, i.e., the construction closes up and ϕ is indeed well defined [Ash et al. 1988].

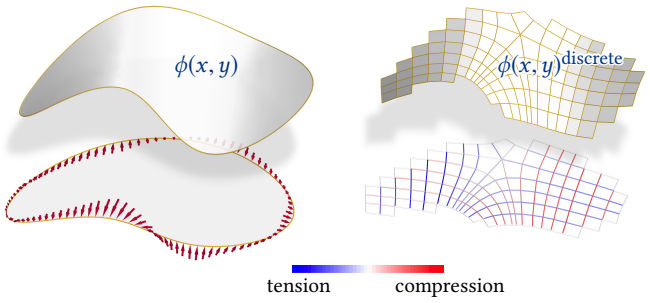

Fig. 7. *Computing an optimal truss in 2D.* Left: Given external forces, we compute an Airy potential $\phi(x, y)$ which minimizes total absolute "isotropic" curvature. Equivalently, we compute a stress state where the integral $\int |\sigma_1| + |\sigma_2|$ of absolute principal stresses is minimal. *Right:* an optimal circular truss is derived form the principal stress directions; it has a corresponding discrete Airy potential. The misalignment with the boundary shows that constraining the vertices of this circular mesh onto the given boundary will impose additional constraints. Later images in this paper show the 3D situation, where these constraints have tacitly been taken into account. Color coding indicates tensile and compressive axial forces.

Step 2. We have established that the Airy potential of a volume-optimal truss minimizes a discrete version of $\int |\kappa_1| + |\kappa_2|$. We therefore switch from discrete to continuous and extend ϕ to the interior of D by minimizing this integral. This optimization problem is solved numerically, using a suitable triangulation of D which is unrelated to the optimal truss, see § 4.2.

Step 3. The eigenvectors of the Hessian of ϕ yields the cross field of i-principal directions on the Airy potential surface. We find a quad mesh aligned with it, using the method of Bommes et al. [2009].

Step 4. According to § 2.2, the mesh extracted in step 3 is approximately circular, and at the same time approximately a volume-optimizing truss. Depending on the property we wish to establish in an exact manner, a final round of optimization is applied, using the method of Tang et al. [2014]. An example is shown by Fig. 7.

3 VOLUME-OPTIMAL STRUCTURES IN 3D

Recently, questions regarding the limit of economy have been asked settings which are more general than the original setup by Michell [1904]. T. Mitchell [2013; 2014] investigated shell-like surfaces discretized by trusses. We build on his work in this paper. Note that Maxwell's lemma and Michell's theorem no longer apply, even if some of their conclusions are still true. This is because the self-load amounts to non-constant forces acting in all interior vertices of the structure.

Our aim is to design volume-optimal surface-like structures. It will be argued why such structures should be based on quadrilateral meshes, and in particular, circular quad meshes. Like in the 2D case, the combinatorics of the structure is part of the solution.

An essential ingredient of our approach is the separation of horizontal forces from vertical ones, so that we are able to treat a *projection* of our structure as an ordinary 2D truss loaded at the boundary, using the methods of § 2.2.

3.1 Mathematical model

The structures treated in this paper are bar-and-joint frameworks. Structural engineering labels do not apply to them without further explanation: In computations they are treated like trusses (no transfer of torque in the joints) but the joints used in the actual structure must be able to withstand torque in order to balance forces other than the deadload. The absence of bending stresses resp. torque in volume-optimal structures is argued by [Mitchell 2013, p. 45] (bending does do not occur, because the constituent material is used more effectively then).

Stresses in membranes, shells, and truss-like continua. Our method requires that we consider a continuous approximation of our discrete structures. In structural engineering, such thin surface-like solids come in various forms and with various mathematical models: plates are flat, shells are curved and experience both axial and bending stresses, while membranes are curved and bending is neglected. The continuous version which applies to our structures is the "truss-like continuum" invented by Michell [1904], see [Whittle 2007]. It has qualities of a membrane in so far as bending stresses are absent. The main difference to the classical shells and membranes is the following: The differential equations governing stresses originate in an infinitesimal balance of forces, but also in the so-called *compatibility* of the strains derived from the stresses via the material's constitutive equations. That compatibility is absent in our case. A truss-like continuum could describe materials composed of fibers, see e.g. Fig. 2, but this is not relevant for the present paper.

Differential-geometric setting. In our setup, the design surface (which guides the optimal structure) is represented as the graph of a function, $z = s(x, y)$. We use x, y as parameters on the surface. A vector $\mathbf{a}$ tangent to the surface in a point $(x, y, s(x, y))$ is described by its projection $\bar{\mathbf{a}}$ onto the xy plane. As usual, scalar products of vectors $\mathbf{a}, \mathbf{b}$ are expressed in terms of $\bar{\mathbf{a}}, \bar{\mathbf{b}}$ and the first fundamental form $\mathbb{I}(x, y)$, cf. [do Carmo 1976]:

$$\langle \mathbf{a}, \mathbf{b} \rangle = \bar{\mathbf{a}}^T \, \mathbb{I} \, \bar{\mathbf{b}}, \text{ where } \mathbb{I} = \begin{pmatrix} 1 + s_{,x}^2 & s_{,x} s_{,y} \\ s_{,x} s_{,y} & 1 + s_{,y}^2 \end{pmatrix}. \tag{7}$$

We use the symbol J for rotation by 90 degrees within the plane which contains the vectors under consideration. Rotation in the xy plane is multiplication with the matrix $J_{xy} = \left(\begin{smallmatrix} 0 & -1 \\ 1 & 0 \end{smallmatrix}\right)$. For vectors $\mathbf{a}, \mathbf{b}$ in the surface's tangent plane, we have the relation $\mathbf{a} = J\mathbf{b} \iff \bar{\mathbf{a}} = \Delta^{-1/2} J_{xy} \mathbb{I} \bar{\mathbf{b}}$, where

$$\Delta = \det \mathbb{I} = 1 + s_{,x}^2 + s_{,y}^2. \tag{8}$$

We note that the area form on the surface is $\sqrt{\Delta}\, dxdy$.

We are further interested in a network of curves on the surface with the property that infinitesimal quadrangles are planar. Our intention is to let the edges of a quad mesh follow these curves and make the faces of that mesh planar. If $\mathbf{a}_1, \mathbf{a}_2$ are tangent to curves of the first resp. second family, then the condition of infinitesimal planarity ("conjugacy", cf. [do Carmo 1976; Liu et al. 2006]) is

$$\bar{\mathbf{a}}_1^T \cdot \nabla^2 s \cdot \bar{\mathbf{a}}_2 = 0. \tag{9}$$

We consider only vertical loads, except at the boundary. This means that projection of the surface together with its stresses into the xy plane yields a 2D domain subject to boundary load, and an ordinary

2D stress tensor $\bar{S}$ in its interior. Analogous to Equ. (5), horizontal equilibrium is expressed by existence of an Airy potential ϕ:

$$\operatorname{div}(\bar{S}) = 0 \iff \hat{\bar{S}} = \nabla^2\phi.$$

Vertical equilibrium

$$\operatorname{div}(\bar{S}\nabla s) = \bar{F}, \quad \text{where} \quad \bar{F} = \sqrt{\Delta}F, \tag{10}$$

involves the load F per surface area, or equivalently, the load $\bar{F}$ per 2D area [Angelillo and Fortunato 2004; Vouga et al. 2012].

The meaning of $\bar{S}$ is the following. In 2D, for any vector $\bar{\mathbf{b}}$, the stress (force-per-length of $\bar{\mathbf{b}}$) in a hypothetical cut orthogonal to $\bar{\mathbf{b}}$ is given by $\bar{S}\bar{\mathbf{b}}$. When working with projections, it is more convenient to compute the projection $\bar{\mathbf{f}}$ of the stress $\mathbf{f}$ (force per length) in a hypothetical cut in the direction *parallel* to some vector $\mathbf{a}$, not orthogonal to it. We get $\bar{\mathbf{f}} = \frac{1}{\|\mathbf{a}\|}\bar{S}J_{xy}\bar{\mathbf{a}}$ and compute the normal stress, i.e., the component of $\mathbf{f}$ orthogonal to the cut:

$$\begin{aligned}\sigma^n &= \left\langle \mathbf{f}, J\frac{\mathbf{a}}{\|\mathbf{a}\|}\right\rangle = \left(\frac{1}{\|\mathbf{a}\|}\bar{S}J_{xy}\bar{\mathbf{a}}\right)^T \mathbb{I}\left(\frac{1}{\sqrt{\Delta}}J_{xy}\mathbb{I}\,\frac{\bar{\mathbf{a}}}{\|\mathbf{a}\|}\right)\\ &= \bar{\mathbf{a}}^T\,\frac{J_{xy}^T\bar{S}\,\mathbb{I}\,J_{xy}\,\mathbb{I}}{\sqrt{\Delta}\,\langle\mathbf{a},\mathbf{a}\rangle}\,\bar{\mathbf{a}} = \frac{\bar{\mathbf{a}}^T\,\sqrt{\Delta}\,\nabla^2\phi\,\bar{\mathbf{a}}}{\bar{\mathbf{a}}^T\,\mathbb{I}\,\bar{\mathbf{a}}}.\end{aligned}$$

For the last equality we have used the relations $\mathbb{I}J_{xy}\mathbb{I} = \Delta J_{xy}$ and $J_{xy}^T\bar{S}J_{xy} = \nabla^2\phi$, which are verified by direct computation.

The extremal values of σ^n are the *principal stresses*. Generally, for any symmetric matrix A and symmetric positive definite matrix B, the extremal values of the quotient $\bar{\mathbf{a}}^TA\bar{\mathbf{a}}\,/\,\bar{\mathbf{a}}^TB\bar{\mathbf{a}}$ are given by the eigenvalues of $B^{-1}A$. Thus the principal stresses are the eigenvalues of $\Delta^{1/2}\,\mathbb{I}^{-1}\nabla^2\phi$, and they are attained if $\bar{\mathbf{a}}$ is an eigenvector. Those eigenvectors $\bar{\mathbf{a}}_1, \bar{\mathbf{a}}_2$ are the projections of vectors $\mathbf{a}_1, \mathbf{a}_2$ which indicate the principal stress directions of the surface. Linear algebra tells us that

$$\bar{\mathbf{a}}_1^T \cdot \mathbb{I} \cdot \bar{\mathbf{a}}_2 = 0, \quad \bar{\mathbf{a}}_1^T \cdot \nabla^2\phi \cdot \bar{\mathbf{a}}_2 = 0.$$

The first relation implies orthogonality of the principal stress directions in the design surface, the second one implies conjugacy of these directions in the stress surface.

Remark. A conjugate curve network on the Airy surface, which has *planar* infinitesimal quadrilaterals, is the continuum version of the edges of an Airy polyhedron. They define both primal edges and the equilibrium forces (dual edges) in them, see § 2.2. Conjugacy thus corresponds to equilibrium. The situation is easiest if the curve network is orthogonal: A curve network which is orthogonal on the design surface, and conjugate on the Airy surface, is an orthogonal network along which equilibrium stresses act. The network defined by the directions of principal stresses has these properties, and since these properties define the network uniquely, we have the conclusion "orthogonality + equilibrium = stress-principality".

3.2 3D Structures at the limit of economy

Properties of optimal shell-like trusses. Neither Maxwell's lemma nor Michell's result of Prop. 2 applies to our discrete structures. However we can identify two scenarios where nevertheless volume minimization amounts to

$$\sum_{\text{members}} |f|\ell \to \min, \tag{11}$$

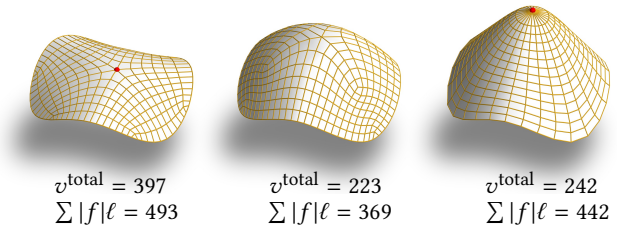

Fig. 8. *User interaction.* We show optimal quad meshes derived without additional constraints (center), and under the constraint that a handle point lies lower (left), resp. higher (right). The effect is demonstrated by means of the value v^{total} of the target functional, and the value $\sum |f|\ell$ of the final structure. In all three cases, FEM analysis confirms that more than 90% of the elastic energy (i.e., the potential energy stored in the structure as the deadload is applied, in the standard load case, with the same boundary conditions as used during optimization) is due to axial forces.

in analogy to Equ. (1). *Scenario 1* is quad mesh combinatorics and a material where tensile limit stress and compressive limit stress are inverses of each other,

$$|\sigma^{\max}| = |\sigma^{\min}|. \tag{12}$$

This is true for steel. We now apply the "faulty" argument mentioned below Proposition 2: In a quad mesh, we have roughly 3/2 times as many linear equilibrium equations as there are forces. Thus the forces are determined by the structure's geometry alone. Each member can be made volume-optimal independent of the others, and is therefore fully stressed. Using the notation from Prop. 2, the structure's total volume then equals $\sum a\ell = \sum |f|/|\sigma|\ell$, where σ is either the tensile or the compressive limit stress. With $|\sigma| = |\sigma^{\min}| = |\sigma^{\max}|$, Equ. (11) follows.

Scenario 2 occurs if the load which is proportional to surface area dominates the unknown weight of the structure, which is subject to optimization. We might think of panel weights of, say, 30 kg/m^2 and maintenance loads of 50 kg/m^2. Snow load might increase the total up to 300 kg/m^2. The steel structure has only 10–30 kg/m^2, and the variation of this weight experienced during optimization is even less. By neglecting this variation we assume the total load is constant during optimization. Then Maxwell's lemma applies, optimal structures are fully stressed, and Equ. (11) holds without assuming quad mesh combinatorics or Equ. (12).

Circular meshes as optimal discrete structures. Many results on volume-optimal 2D trusses are known, but in our setting (surface-like structures) the corresponding statements have not been proved. In the strict mathematical sense, we do not know if in the continuous limit, infinitesimal members are orthogonal, or if, in the discrete case, members form a circular quad mesh. One can argue why analogous statements should hold nevertheless. By letting discrete optimal trusses converge to a continuous truss-like structure, the following conclusions are drawn by [Mitchell 2013, §§9–10]:

- Stresses in an optimal continuum obey literally the same equations as stresses in a membrane.
- The principal directions of stress coincide with the principal directions of curvature.

Consequently we use *circular quad meshes* as discrete versions of such structures.

This choice remains valid even if do not make the assumptions from which the above conclusions have been inferred. Firstly an optimal truss should follow the principal stress directions in order to optimally utilize the material, at least where there is both tension and compression (this implies quad mesh combinatorics and orthogonality of edges). Secondly, the conclusions about quad mesh combinatorics and orthogonality follow automatically from Prop. 3, if scenario 2 is adopted. Planar faces are an additional requirement which comes from entirely practical considerations, namely enabling flat panels. Now orthogonality together with planarity implies that the bars of our optimal structure should represent a discrete version of the principal curvature lines. Since all possible discretizations of principal curvature lines (including in particular circular meshes) are close together [Liu et al. 2006] it is no additional restriction to require circular meshes.

Properties of optimal continua. In our optimization, we need a continuous version of Equ. (11). Suppose that principal stresses σ_1^n, σ_2^n act parallel to the sides of an infinitesimal rectangular surface element of dimensions $d\ell_1 \times d\ell_2$. The total "force" in the first direction is $\sigma_1\, d\ell_2$, the length of fibers being $d\ell_1$. With a similar statement for the 2nd direction, this surface element contributes the amount $(|\sigma_1^n| + |\sigma_2^n|)d\ell_1\, d\ell_2$ to $\sum |f|\ell$. This sum therefore corresponds to the surface integral of $|\sigma_1^n| + |\sigma_2^n|$.

Recall that principal stresses are eigenvalues of $\Delta^{1/2}\, \mathbb{I}^{-1}\nabla^2\phi$, and that the surface element in xy coordinates is $\Delta^{1/2}\, dxdy$. We therefore have the following continuous version of Equ. (11):

$$\sum_{\substack{\text{infinitesimal}\\ \text{members}}} |f|\ell \approx \iint (|\lambda_1| + |\lambda_2|)\, \Delta\, dx\, dy \to \min, \qquad \lambda_1, \lambda_2 \text{ eigenvalues of } \mathbb{I}^{-1}\nabla^2\phi. \tag{13}$$

Remark. If Equ. (13) had $\Delta^{1/2}$ instead of Δ, then it would express minimization of a certain total absolute curvature, similar to the 2D case. This is because λ_1, λ_2 are the *i*-curvatures of the Airy surface $z = \phi(x, y)$ w.r.t. the first fundamental form of the design surface.

3.3 Computing optimal structures – the workflow

The preparations above enable us to compute optimal discrete structures which have the shape of shells, see Fig. 6. This procedure is similar to the one presented in § 2.3 for the 2D case. Note that the combinatorics of the structure is part of the solution.

We solve the following problem: *Given boundary conditions, find a shell-like truss which (i) balances self-loads and exterior boundary forces; (ii) observes geometric boundary conditions; and (iii) is volume-optimal.* The procedure consists of the following steps:

Step 1: Form and force optimization. We set up an optimization problem for an Airy potential function $\phi(x, y)$ and a design surface $z = s(x, y)$. The optimization target is Equ. (13). Constraints include the user-defined ones, and the ones arising from the relations between ϕ and s. In addition we require that the principal stress directions are conjugate w.r.t. the design surface — otherwise the faces of the final truss cannot be planar. Numerical optimization is performed over a suitable triangulation which is unrelated to the optimal truss. It requires an elaborate setup of variables and constraints, see § 4.1.

Step 2: Meshing. Using the *mixed integer quadrangulation* method of Bommes et al. [2009], we extract a quad mesh which follows the cross field of principal directions in the design surface.

Step 3: Post-Processing. A round of optimization make faces planar and puts forces into equilibrium, which is exactly the problem solved by Tang et al. [2014]. Postprocessing may of course vary from example to example. Finally, an engineering task is performed: an actual structure is planned on basis of that mesh. The cross-sections of members are chosen on basis of the forces we computed, such that the member has minimal weight (taking a safety margin into account). Joints and foundations are modeled, and the structure undergoes FEM testing for standard load cases (which is not part of this paper). Note that the members' weight influences the load, so these members must be implicitly present already during Step 1.

4 IMPLEMENTATION

This section describes in detail the first stage in our workflow for computing optimal structures, namely finding an optimal design surface $z = s(x, y)$ together with its stress potential $\phi(x, y)$. The 2D case is treated briefly afterwards.

4.1 Variables and constraints for optimal shells

Setup of variables. We describe the design surface $z = s(x, y)$ as graph over a planar domain which is given as a triangle mesh. Each vertex is associated with a coordinate vector $\bar{\mathbf{v}} = (v_1, v_2) \in \mathbb{R}^2$ (fixed), the design surface's z coordinate $v_3 = s(\bar{\mathbf{v}})$ which is subject to optimization, and the following additional variables.

- gradient ∇s and Hessian $\nabla^2 s$ (5 variables)
- 2nd derivatives $\phi_{,xx}, \phi_{,xy}, \phi_{,yy}$ of the Airy potential, and their derivatives $\phi_{,xxx}, \phi_{,xxy}, \ldots$ (9 variables)
- matrix $\mathbb{I}$, values $\Delta = \det \mathbb{I}$, $\delta = \sqrt{\Delta}$, $\omega = \sqrt{\delta}$ (6 variables)
- eigenvalues λ_1, λ_2 of $\mathbb{I}^{-1}\nabla^2\phi$, their product λ, and principal stresses σ_1, σ_2 (5 variables)
- eigenvectors $\bar{\mathbf{a}}_j$ and vectors $\bar{\mathbf{b}}_j, \bar{\mathbf{c}}_j$ described below (12 var.).

We also have the following constants:

- panel weight ρ in kg/m^3 and panel thickness h.
- The future members of the truss are fully stressed, so their weight can already be computed while we are still optimizing the surface, using Equ. (13): The weight per 2D area element is $\mu(|\lambda_1| + |\lambda_2|)\Delta$, where μ is a constant of dimension m^{-1}.

Constraints. The variables introduced above obey constraints, starting with relations between derivatives and function values. For any of the functions $\psi \in \{\phi_{,xx}, \phi_{,xy}, \phi_{,yy}\}$ the first derivatives are variables in the optimization, and for s we even involve second derivatives. For each pair $\bar{\mathbf{v}}\bar{\mathbf{w}}$ of adjacent vertices, we require

$$s(\bar{\mathbf{w}}) - s(\bar{\mathbf{v}}) = \nabla s(\bar{\mathbf{v}})^T \cdot (\bar{\mathbf{w}} - \bar{\mathbf{v}}) + \tfrac{1}{2}(\bar{\mathbf{w}} - \bar{\mathbf{v}})^T \cdot \nabla^2 s(\bar{\mathbf{v}}) \cdot (\bar{\mathbf{w}} - \bar{\mathbf{v}}),$$
$$\psi(\bar{\mathbf{w}}) - \psi(\bar{\mathbf{v}}) = \nabla\psi(\bar{\mathbf{v}})^T \cdot (\bar{\mathbf{w}} - \bar{\mathbf{v}}), \quad \text{for } \psi \in \{\phi_{,xx}, \phi_{,xy}, \phi_{,yy}\}.$$

As $\bar{\mathbf{w}}$ runs through the 1-ring or 2-ring neighbourhood of $\mathbf{v}$ (depending on whether we want to compute 1st or 1st+2nd derivatives) the above equations constitute an over-determined linear system of the form "$MX = B$" for the vector X of derivatives at $\bar{\mathbf{v}}$. It is solved by

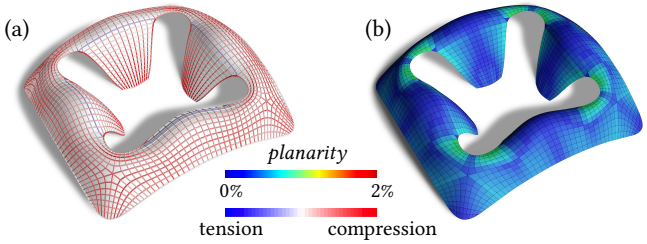

Fig. 9. *Boundary conditions.* Parts of the boundary of this steel-glass structure are physically supported, others are free. During optimization, however, all boundaries have prescribed x, y coordinates in order to preserve the design intent. (a), (b) show tension and compression in the final structure, and planarity of faces.

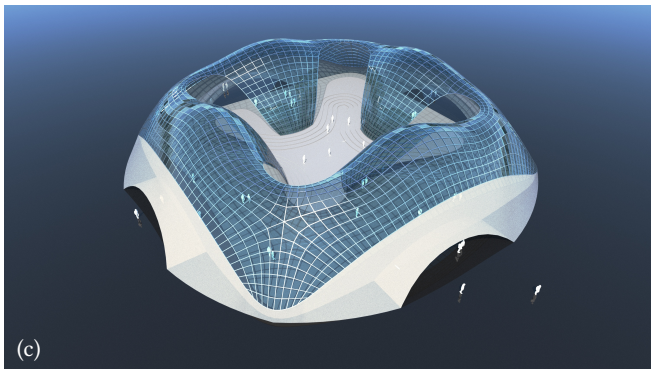

minimizing $\|MX - B\|^2$. This expression's derivatives w.r.t. both X and B must vanish, since both X, B are variables in our optimization, This leads to

$$M^T MX = M^T B, \quad MX = B. \tag{14}$$

The size of M depends on the size of the neighbourhood, but for the purpose of counting the number of constraints vs. the number of variables, we consider the balance even. The constraint sets C_1 and C_2 obtained in this way refer to derivatives of design surface and stress surface, resp. Further, for each vertex we have the following sets $C_3, \ldots, C_8$ of linear or quadratic constraints:

- C_3 Derivatives obey $\phi_{,xxy} = \phi_{,xyx}$ and $\phi_{,xyy} = \phi_{,yyx}$.
- C_4 Equations (7), (8) define $\mathbb{I}, \Delta$. We require $\delta^2 = \Delta$, $\omega^2 = \delta$ in order to ensure a positive square root of Δ (6 constraints).
- C_5 The defining relations $\lambda_1 + \lambda_2 = \mathrm{tr}(\mathbb{I}^{-1}\nabla^2\phi)$, $\lambda_1\lambda_2 = \det \nabla^2\phi / \det \mathbb{I}$ are made quadratic by multiplication of both l.h.s. and r.h.s. with Δ, and the substitution $\lambda = \lambda_1\lambda_2$. Stresses are defined by $\delta\sigma_i = \lambda_i$, $i = 1, 2$ (5 constraints).
- C_6 The defining relations $\nabla^2\phi \cdot \bar{\mathbf{a}}_i = \lambda_i \mathbb{I}\bar{\mathbf{a}}_i$ of the principal stress directions are made quadratic by the substitution $\mathbb{I}\bar{\mathbf{a}}_i = \bar{\mathbf{b}}_i$. We further require $\bar{\mathbf{a}}_i^T\bar{\mathbf{a}}_i = 1$ and $\bar{\mathbf{a}}_1^T\bar{\mathbf{b}}_2 = \bar{\mathbf{a}}_2^T\bar{\mathbf{b}}_1 = 0$ to be sure to pick an orthonormal basis of eigenvectors.
- C_7 Equ. (9), substituting $\bar{\mathbf{c}}_i = \nabla^2 s \cdot \bar{\mathbf{a}}_i$, makes 5 constraints.

Note that $|C_6| = 5$: Computing eigenvectors is 2 equations, normalization amounts to another 2, and orthogonality constraints for eigenvectors can be omitted in a d.o.f. count. Constraint set C_8 consists of the equilibrium equation (10). It expands to $\bar{F} = s_{,xx}\phi_{,yy} - 2s_{,xy}\phi_{,xy} + s_{,yy}\phi_{,xx}$, where the load $\bar{F}$ is the structure's weight plus the panel weight, leading to $\bar{F} = \mu(|\lambda_1| + |\lambda_2|)\Delta + \rho h\delta$. This equation involves absolute values and is approached by the method of iteratively reweighted least squares: At iteration level k, $|\lambda_i|$ is replaced by

$$|\lambda_i| = w_{i,k}\lambda_i^2, \text{ where } w_{i,k} = 1 \,/\, \sqrt{(\lambda_{i,k-1})^2 + \epsilon}. \tag{15}$$

Here $\epsilon > 0$ is a small regularizer, and $\lambda_{1,k-1}, \lambda_{2,k-1}$ are constants equal to the value of λ_1, λ_2 in the previous iteration. With this substitution, the equilibrium equation becomes quadratic. This concludes the enumeration of constraints per vertex.

Boundaries. The x, y coordinate of all vertices are fixed. The z coordinates $s(\bar{\mathbf{v}})$ of vertices are typically free. At the boundary we can opt for fixed or for free z coordinates. A different property of a boundary vertex is if it is physically supported or free, see e.g. Figure 9. An unsupported part of the shell's boundary experiences no external forces except the deadload. The corresponding boundary part of the Airy potential lies in a plane [Miki et al. 2015], but in our optimization we compute with the condition $\bar{\mathbf{n}}^T\mathbb{I}\bar{S}\nabla s = 0$, where $\bar{\mathbf{n}}$ is an outer normal of the boundary, cf. [Vouga et al. 2012]. Figure 10 gives an overview of the different boundary conditions we use.

Counting degrees of freedom. Let us first discuss the continuous case in a naive way. If the design surface $z = s(x, y)$ is given, the stress potential $\phi(x, y)$ is found by the equilibrium condition (10), which is a 2nd order PDE. It is elliptic in case stresses are all compressive [Vouga et al. 2012], so ϕ is uniquely determined by boundary values. Even if we have a mixture of tensile and compressive stresses we expect the same behaviour. The requirement that principal stress directions agree with principal curvature directions is again a 2nd order PDE, so we can expect that both s and ϕ are determined by boundary values. Any further constraint, like requiring that a boundary is a principal curve, leads to loss of freedom for the boundary of the design surface. For volume optimization not much freedom is left now – we basically only have the boundary values of ϕ at our disposal.

In the discrete setting we have one constraint per vertex less than there are variables, if we disregard Equation (9) which enforces alignment of principal stress directions with principal curvature directions. This is in accordance with the fact that for a given design

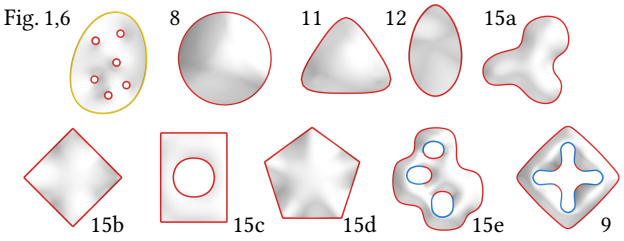

Fig. 10. Boundary conditions imposed on the examples contained in this paper. The manner of condition along the boundary is indicated by colors: red is physically supported with fixed z coordinate, yellow is supported with free z coordinate, blue is unsupported with free z coordinate.

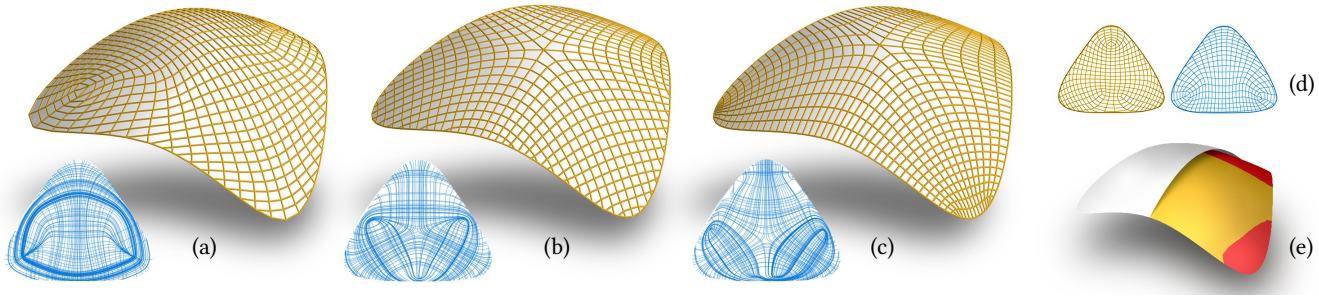

Fig. 11. *Comparing optimization with and without alignment constraints.* Optimization and quad meshing guided by principal stress directions (inset figures) yields different meshes, if optimization is performed subject to different constraints: (a) without alignment of principal stresses and principal curvatures, (b) with this alignment, using Equ. (9) (c) in addition, alignment of principal curves with the boundary. Subfigure (d) shows the discrepancy between principal stress directions and principal curvature directions in the first case, and subfigure (e) shows the 3 design surfaces superimposed (a=white, b=red, c=yellow), from which we conclude that the difference in these three meshes is mainly the combinatorics, not the geometric shape.

surface, the stress potential is determined. Enforcing Equ. (9) leads to as many equations as there are variables, implying that no degrees of freedom are left. This is in accordance with the shape restriction we already saw in the continuous case, and it means that enforcing this condition makes our optimization procedure a tool for form-finding.

Target functional for optimization. It is not difficult to express the target functional of Equ. (13) in terms of our variables. Recall that we work with a triangulation of a planar domain. Each vertex $\bar{\mathbf{v}}$ has an area of influence $A(\bar{\mathbf{v}})$, which is computed as one third of the area of its vertex star. In the k-th round of our iterative optimization procedure, volume minimization is then expressed by

$$\begin{aligned}\sum_{\substack{\text{infinitesimal}\\ \text{members}}} |f|\ell &\approx \iint (|\lambda_1| + |\lambda_2|)\,\Delta\, dx\, dy \\ &\approx \sum\nolimits_{\text{vertices}} (w_1^k \lambda_1^2 + w_2^k \lambda_2^2)\Delta A \\ &= \sum\nolimits_{\text{vertices}} (w_1^k \sigma_1^2 + w_2^k \sigma_2^2) A \to \min . \end{aligned} \tag{16}$$

All expressions are values associated with vertices; recall the weights w_i^k from Equ. (15). This is a quadratic objective function.

Further constraints. Several of the results shown in this paper add more constraints to the optimization, like handles operated by the designer (Fig. 8), or proximity to a reference surface, which can be treated as quadratic constraints [Tang et al. 2014]. A particular constraint highly relevant to architectural design is alignment of the mesh with the given boundary (see examples in Figures 6, 8, 9 and the comparison in Fig. 11). With $\bar{\mathbf{t}}$ as a (projected) tangent vector at the boundary, and $\bar{\mathbf{a}}_1, \bar{\mathbf{a}}_2$ as the principal stress vectors, constraint set C_7 is augmented by $(\bar{\mathbf{t}}^T \mathbb{I}\, \bar{\mathbf{a}}_1) \cdot (\bar{\mathbf{t}}^T \mathbb{I}\, \bar{\mathbf{a}}_2) = 0$. Unfortunately this constraint can almost never be fulfilled exactly — a closed curve (like the boundary) can be a principal curvature line only if the integral of torsion is an integer multiple of 2π. This can be achieved if the z coordinates of boundary vertices are free variables in our optimization, but otherwise this obstruction has the effect that near the boundary, the angles in our mesh deviate from 90 degrees, see Figures 9c, Fig. 15b, and Fig. 15e.

Optimization by guided projection. The target functional (13) resp. (16) is optimized by the constraint solver by Tang et al. [2014], which works best for systems of linear or quadratic constraints, each involving only few variables. The method tries to move the vector of variables towards the constraint manifold, such that the path is guided by a quadratic energy. In our case, the energy is provided by the quadratic objective function (16). Statistics are shown by Fig. 13.

4.2 Variables and constraints for optimal 2D trusses

The procedure for optimizing shell-like trusses described in § 4.1 specializes to the 2D case if we let s and its derivatives equal zero, and let the self-weight be zero. Then $\mathbb{I}$ becomes the unit matrix, and $\Delta = \delta = \omega = 1$. The eigenvalues λ_i become the curvatures κ_i needed for the target functional. In this way many variables and constraints disappear. Further we can drop the conjugacy condition (9). The rest is unchanged, and we do not elaborate further.

5 DISCUSSION

We start the discussion with several different instances of the optimization procedure proposed in this paper. Fig. 11 compares optimization with and without enforcing Equ. (9), i.e., disregarding alignment of principal stress directions with principal curvature directions. It is encouraging to see that the design surface is almost unchanged, see superimposed surfaces in Fig. 11e. We see that Equ. (9) does not prevent optimization for minimal weight.

Verification of results. We measure the success of our optimization procedures in different ways. Firstly, measuring planarity of faces is straightforward (see individual images). Secondly, our working assumption to treat shells as membranes is verified a posteriori by FEM analysis of structures with rigid joints based on the meshes we generate: In our examples, more than 90% of the elastic energy in the basic load case is due to axial forces.

Thirdly, we compare structures derived from optimized meshes with structures derived from meshes obtained in another way, see Fig. 12. Numerical experiments confirm that in non-optimized meshes, axial forces typically are 2–3 times larger, and the weight of the structure is about 50% bigger. These experiments measure the effect of our optimization. Another comparison is shown by Figure 8, where we demonstrate how a user's interference with free optimization causes the weight of the final structure to increase.

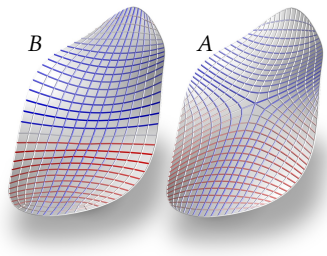

	A	B	
max $\|f\|$	74	202	[kN]
moment	1.9	6.7	[kNm]
weight	8100	12900	[kg]
$\sum \|f\|\ell$	$40{\cdot}10^3$	$53{\cdot}10^3$	[kNm]

Fig. 12. *Effectiveness.* We compare meshes with the same boundary: Mesh A is optimized according to § 4.1, while mesh B is computed by minimizing a fairness energy and subsequent quad meshing. They undergo postprocessing by optimization for equilibrium and planar faces according to [Tang et al. 2014], and subsequent modeling of a structure with rigid joints. The members' cross-sections are selected according to maximum allowable stresses and maximum allowable displacement. Then structure B is 60% heavier than structure A, and the effect is even bigger if we skip the maximum displacement requirement. The underlying surfaces are very similar, confirming the big influence of the structure's combinatorics (and the positioning of members) on the weight.

Fig.	1,6	9	12	15a	15b	15c	15d	15e
$\|V\|$	1082	1865	882	678	673	973	1133	2003
$\|F\|$	2026	3403	1662	1254	1252	1772	2149	3712
# of variables	41 k	89 k	33 k	25 k	25k	36 k	16k	96 k
# of constraints	73 k	228 k	68 k	51 k	51k	73 k	32k	238 k
time [sec]	325	265	16	35	19	60	42	338
weights given to individual constraints, ordered by constraint set								
target functional	10^{-5}	10^{-8}	10^{-4}	10^{-4}	10^{-4}	10^{-2}	10^{-3}	10^{-6}
C_1,C_2,C_3	400,10^2,40	1,1,1	2,1,1	2,1,1	1,1,1	2,2,2	1,1,1	1,1,1.4
C_4,C_5,C_8	10^2,10^3,200	1,1,2.4	2,1,1	2,1,1	1,1,1	2,2,2	1,1,1	1,1,1.4
C_6,C_7	200,1	1.4,.01	1,1	1,1	1,1	2,1	1,1	1.4,.01
RMS residuals of constraints, ordered by constraint set								
C_1 (derivatives s)	.017	.081	.005	.006	.014	.004	.007	.081
C_2 (derivatives ϕ)	.019	.015	.009	.010	.013	.002	.005	.017
C_3 ($\partial_{xy} = \partial_{yx}$)	.021	.005	.001	.003	.002	.000	.001	.005
C_4 ($\mathbb{I}$, Δ, . . .)	.006	.006	.001	.001	.004	.001	.001	.001
C_5 (eigenvalues)	.012	.001	.000	.010	.011	.000	.000	.012
C_6 (eigenvectors)	.002	.730	.002	.004	.003	.001	.001	.005
C_7 (alignment)	.039	.012	.004	.009	.003	.003	.001	.416
C_8 (equilibrium)	.016	.005	.003	.008	.005	.000	.001	.019

Fig. 13. Details concerning form+stress optimization on a triangle mesh (V, E, F). The large number of constraints appears to contradict § 4.1, but is due to the many equations of type (14). The weights given to constraints and the target functional refer to the method of Tang et al. [2014].

Random experiment	GP_1	I_1	GP_2	I_2	GP_3	I_3	GP_4	I_4
time [sec]	0.18	145	0.14	101	0.15	160	0.14	139
target functional	10.8	9.75	12.7	11.4	13.3	11.8	6.62	5.90
distance	0.03		0.03		0.04		0.02	

Fig. 14. We compare our "guided projection" method with the constrained solver of [Wächter and Biegler 2006]. Columns "GP" and "I" refer to 10 rounds of either method. We perform optimization according to § 4.2 on four meshes with 1600 vertices and randomly generated boundary (9444 variables, 8000 constraints). We show runtime, the value of the target functional, and the distance between the resulting surfaces. The final designs achieved with the two methods are very different.

Implementation details. Figure 13 gives details on computation times for the optimization process described by § 4.1. For meshing and post-meshing optimization, which are no contributions of this paper, we refer to [Bommes et al. 2009] and [Tang et al. 2014], respectively. The times given are for an Intel Core i5-6500 CPU with 3.20GHz and 15.6 GB memory.

A word about the nature of our optimization procedure is in order. The guided projection method of Tang et al. [2014] does not exactly *minimize* the target functional, but use this functional to guide a mesh towards the solution manifold defined by the constraints (one could achieve minimization by adjusting weights as the iteration progresses). Fig. 14 shows comparisons with a constrained solver. Numerical experiments show that apart from some outliers, already after 10 iterations our method minimizes the target within a margin of 10–12%, but computation is faster by orders of magnitude. We stayed with our method because we expect that in an architectural design situation, exact minimization does not have priority. The reason for this is not only the desire for design freedom, but also the additional constraints and safety requirements an actual structure is required to conform to, and which cause some discrepancy between the optimized mesh and the structure based on it (see e.g. maximum displacement constraint in Fig. 12).

Limitations, Robustness. Some of the constraints and optimization targets discussed in this paper are conflicting. We have pointed out where a designer's wishes might not be able to be fulfilled, e.g. when a fixed boundary curve is expected to be aligned with a principal direction. The main limitation of the methods presented in this paper therefore lies in understanding the effect of side conditions. They must be balanced by weighting, which is the designer's choice. So far we have an academic implementation of our procedures which requires some experience in correctly setting the weights, cf. Fig. 13.

When computing with curvatures (and generally, higher derivatives), robustness is always an issue. We should should add that we did not experience problems here, since the principal directions of our shapes are variables in our optimization procedure and are thus automatically subject to its regularizing effect.regularization.

Future Research. The interpretation of volume-minimization as minimization of kinks on the stress polyhedron (in the sense of isotropic geometry) immediately leads us to ask the same question in Euclidean geometry. The sum $\sum \ell|\alpha|$ of length times kink angle over all edges of a mesh can be seen as a fairness measure which discretizes the total absolute curvature $\int |\kappa_1| + |\kappa_2|$. We conjecture that the kink-minimal meshing of a given design surface will lead to a principal mesh in negatively curved areas. Finding such meshes for a given boundary can probably be done in a way similar to this paper. Another direction of future research is a systematic study of optimization problems which exhibit both a discrete and a continuous version, especially network optimization and their applications, cf. [Whittle 2007].

ACKNOWLEDGMENTS

This research was supported by SFB-Transregio programme *Geometry and Discretization* (Austrian Science Fund grant no. I 2978), and by the project "Geometry and Computational Design for Architecture and Fabrication" at Vienna University of Technology. Special thanks go to Heinz Schmiedhofer for help with the illustrations.

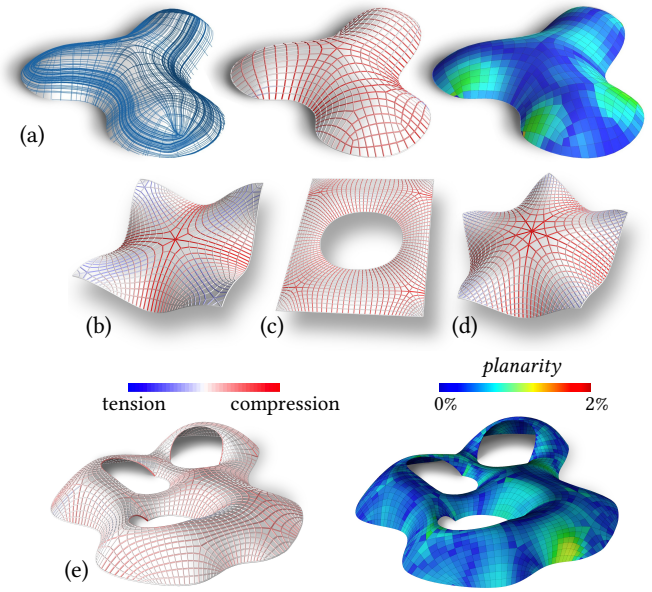

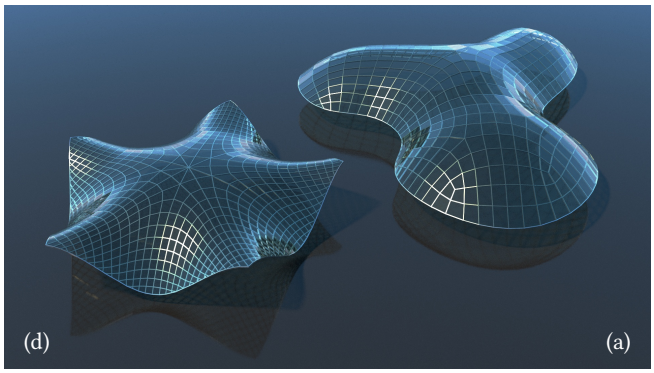

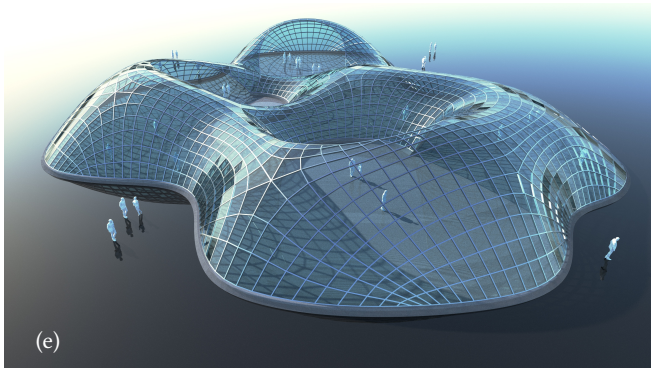

Fig. 15. Examples of optimal structures, (a)–(e). We show tensile and compressive forces in structures derived from optimized meshes. For examples (a), (e) also the optimal shape with principal stress lines and the planarity of the quad mesh derived from it are shown. Structures (b,e) have been optimized with the additional constraint of alignment with the fixed boundary. We hit the "integral of torsion" obstruction mentioned in § 4.1, so the angle between edges visibly deviates from 90 degrees.

REFERENCES

Niels Aage, Oded Amir, Anders Clausen, Lior Hadar, Dana Maier, and Asbjørn Søndergaard. 2015. Advanced Topology Optimization Methods for Conceptual Architectural Design. In *Advances in Architectural Geometry 2014*, Philippe Block et al. (Eds.). Springer.

Sigrid Adriaenssens, Philippe Block, Diederik Veenendaal, and Chris Williams (Eds.). 2014. *Shell Structures for Architecture.* Taylor & Francis.

Maurizio Angelillo and Antonio Fortunato. 2004. Equilibrium of masonry vaults. In *Novel Approaches in Civil Engineering*, M. Frémont et al. (Eds.). Springer, 106–111.

Peter Ash, Ethan Bolker, Henry Crapo, and Walter Whiteley. 1988. Convex polyhedra, Dirichlet tessellations, and spider webs. In *Shaping space.* Birkhäuser, 231–250.

William F. Baker, Lauren L. Beghini, Arkadiusz Mazurek, Juan Carrion, and Alessandro Behini. 2013. Maxwell's reciprocal diagrams and discrete Michell frames. *Struct. Multidisc. Optim.* 48 (2013), 267–277.

Kai-Uwe Bletzinger and Ekkehard Ramm. 1993. Form Finding of Shells by Structural Optimization. *Engineering with Computers* 9, 1 (1993), 27–35.

Phillipe Block and John Ochsendorf. 2007. Thrust Network Analysis: A New Methodology For Three-Dimensional Equilibrium. *J. Int. Assoc. Shell and Spatial Structures* 48, 3 (2007), 167–173.

Alexander Bobenko and Yuri Suris. 2009. *Discrete differential geometry: Integrable Structure.* American Math. Soc.

David Bommes, Henrik Zimmer, and Leif Kobbelt. 2009. Mixed-integer Quadrangulation. *ACM Trans. Graph.* 28, 3 (2009), #77.

Manfredo do Carmo. 1976. *Differential Geometry of Curves and Surfaces.* Prentice-Hall.

Fernando Fraternali. 2010. A thrust network approach to the equilibrium problem of unreinforced masonry vaults via polyhedral stress functions. *Mechanics Res. Comm.* 37 (2010), 198–204.

Fernando de Goes, Pierre Alliez, Houman Owhadi, and Mathieu Desbrun. 2013. On the Equilibrium of Simplicial Masonry Structures. *ACM Trans. Graph.* 32, 4 (2013), #93.

Daniel G. Goetschel. 1981. On the derivation of Michell's theorem. *Mechanics Res. Comm.* 8, 5 (1981), 319–322.

Caigui Jiang, Chengcheng Tang, Hans-Peter Seidel, and Peter Wonka. 2017. Design and Volume Optimization of Space Structures. *ACM Trans. Graphics* 36, 4 (2017), #159.

Yang Liu, Helmut Pottmann, Johannes Wallner, Yong-Liang Yang, and Wenping Wang. 2006. Geometric modeling with conical meshes and developable surfaces. *ACM Trans. Graphics* 25, 3 (2006), 681–689.

James C. Maxwell. 1872. On reciprocal figures, frames, and diagrams of forces. *Trans. R. Soc. Edinburgh* 26 (1872), 1–40.

Anthony G. M. Michell. 1904. The limit of Economy of Material in Frame-structures. *Phil. Mag., Ser. VI* 8 (1904), 589–597.

Masaaki Miki, Takeo Igarashi, and Philippe Block. 2015. Parametric Self-supporting Surfaces via Direct Computation of Airy Stress Functions. *ACM Trans. Graph.* 34, 4 (2015), #89.

Toby Mitchell. 2013. *A limit of economy of material in shell structures.* Ph.D. Dissertation. Univ. California, Berkeley. `http://escholarship.org/uc/item/0m72v2tt`.

Toby Mitchell. 2014. A limit of economy of material in shell structures. In *Membranes and Spatial Structures: Footprints.* P. 309. [IASS-SLTE Symposium].

Daniele Panozzo, Philippe Block, and Olga Sorkine-Hornung. 2013. Designing Unreinforced Masonry Models. *ACM Trans. Graph.* 32, 4 (2013), #91.

Edward W. Parkes. 1965. *Braced Frameworks.* Pergamon Press.

Helmut Pottmann, Michael Eigensatz, Amir Vaxman, and Johannes Wallner. 2015. Architectural Geometry. *Computers and Graphics* 47 (2015), 145–164.

Helmut Pottmann and Yang Liu. 2007. Discrete Surfaces in Isotropic Geometry. In *Mathematics of Surfaces XII.* Springer, 431–363.

William Prager. 1978. Nearly Optimal Design of Trusses. *Computers & Structures* 8 (1978), 451–454.

Alexander Schiftner and Jonathan Balzer. 2010. Statics-Sensitive Layout of Planar Quadrilateral Meshes. In *Advances in Architectural Geometry 2010*, Cristiano Ceccato et al. (Eds.). Springer, 221–236.

David J. Steigmann and Allen C. Pipkin. 1991. Equilibrium of Elastic Nets. *Phil. Trans. R. Soc. Lond. A* 335 (1991), 419–454.

Karl Strubecker. 1962. Airy'sche Spannungsfunktion und isotrope Differentialgeometrie. *Math. Zeitschrift* 78 (1962), 189–198.

Chengcheng Tang, Xiang Sun, Alexandra Gomes, Johannes Wallner, and Helmut Pottmann. 2014. Form-finding with Polyhedral Meshes Made Simple. *ACM Trans. Graphics* 33, 4 (2014), #70.

Etienne Vouga, Mathias Höbinger, Johannes Wallner, and Helmut Pottmann. 2012. Design of Self-Supporting surfaces. *ACM Trans. Graphics* 31, 4 (2012), #87.

Andreas Wächter and Lorenz T. Biegler. 2006. On the Implementation of a Primal-Dual Interior Point Filter Line Search Algorithm for Large-Scale Nonlinear Programming. *Math. Progr.* 106 (2006), 25–57.

Peter Whittle. 2007. *Networks – Optimisation and Evolution.* Cambridge Univ. Press.

Julius Wolff. 1892. *Das Gesetz der Transformation der Knochen.* Hirschwald, Berlin.